



Robust Room Temperature Superparamagnetic Properties of ZnO Nanostructures: Li-Based Fe Dual Dopants

A. M. Youssef¹ · S. M. Yakout¹

Received: 4 June 2021 / Accepted: 13 July 2021 / Published online: 30 August 2021

© The Author(s), under exclusive licence to Springer Science+Business Media, LLC, part of Springer Nature 2021

Abstract

Strong room temperature superparamagnetic properties have been achieved in $\text{Zn}_{0.94}\text{Li}_{0.03}\text{Fe}_{0.03}\text{O}$ nanoparticles within a magnetic field of $\pm 20,000$ Oe. High-purity ZnO, $\text{Zn}_{0.97}\text{Li}_{0.03}\text{O}$, $\text{Zn}_{0.94}\text{Li}_{0.03}\text{Mn}_{0.03}\text{O}$, and $\text{Zn}_{0.94}\text{Li}_{0.03}\text{Fe}_{0.03}\text{O}$ nanostructures were synthesized by means of the coprecipitation method. The XRD crystallographic planes and HRTEM of the synthesized compositions showed that a single phase of a ZnO hexagonal wurtzite structure was obtained with the absence of any secondary phases or magnetic cluster. Pure ZnO powders show asymmetrical nanoparticles with a certain degree of agglomeration and approximately have an average particle size of 37 nm. The TEM image of Li-monodoped ZnO powders displays uniform spherical nanoparticles with less agglomeration, and the average particle size was reduced to 35 nm. The image of the (Li, Mn) codoped ZnO sample illustrates that the particles of ZnO are transformed to elongated shapes without agglomeration with an average particle size of 32 nm. In case of (Li, Fe) codoped ZnO powders, the image clearly shows a mixture of uniform nanospherical and elongated particles with a small average particle size of 27 nm. The absorption edge of ZnO is red shifted to more wavelength absorption due to (Li, Mn) and (Li, Fe) codoping, and it becomes sharper after Li monodoping which is a dynamic factor in the optoelectronic applications. Interestingly, the $\text{Zn}_{0.94}\text{Li}_{0.03}\text{Fe}_{0.03}\text{O}$ composition exhibits a superparamagnetic behavior at room temperature; it obviously shows a semi-saturation magnetization of 0.02 emu/g but has a nearly very small coercivity of 14 Oe. The instantaneous presence of both ferromagnetism and antiferromagnetism in $\text{Zn}_{0.94}\text{Li}_{0.03}\text{Fe}_{0.03}\text{O}$ gives rise to the disordered state of superparamagnetism.

Keywords ZnO nanostructures · (Li Mn) and (Li Fe) codoped ZnO · Room temperature superparamagnetism

1 Introduction

Manipulation of optical, electrical, and magnetic properties in nanostructured semiconductor oxides is an essential step for modern applications such as full-spectrum photocatalysis [1], spintronics [2], magnetic gas sensor [3], solar cell [4], and biomedical [5] applications. Nowadays, the room temperature ferromagnetic and superparamagnetic properties of metal oxide semiconductors have received great attention in the last years [6–10]. Among different metal oxide nanomaterials, zinc oxide (ZnO) is of exceptional interest due to many encouraging properties such as large exciton binding energy of 60 meV and a wide direct band gap of

3.37 eV [11, 12]. ZnO is a natural n-type semiconductor and possesses the richest family of nanostructures [13]. In this regard, ZnO is one of the most promising materials with strong candidates for magnetic-based spintronics and medical applications [6, 10]. In order to modify the physical and chemical properties of ZnO nanostructures, in-depth understanding of its structural, magnetic, and electrical properties is essential. Different magnetic behaviors such as room temperature ferromagnetic and superparamagnetic have been studied and reported for ZnO [14, 15]. Lately, the room temperature superparamagnetic properties are of countless interest due to the standpoints of their use in magnetic resonance imaging (MRI), magnetically guided drug delivery, radiotherapy in vivo, cell DNA, protein separation, magnetic microsensors, and hyperthermia [16]. ZnO is an appropriate material for biomedical applications due to the bio-save, bio-compatibility, nano size, easy preparation, non-toxicity, different morphologies, and low production costs [16]. The modification of ZnO nanostructures by doping or codoping

✉ S. M. Yakout
s_mabrok2002@yahoo.com

¹ Inorganic Chemistry Department, National Research Centre (NRC), El Buhouth St, Dokki, Cairo 12622, Postal Code, Egypt

with special transition metal and nonmetal elements makes it possible to enhance the electrical, magnetic, and optical properties of materials by changing the bulk and surface properties [17–23]. For ZnO, Li^+ (0.78 Å), Mn^{2+} (0.67 Å), Fe^{2+} (0.61 Å), and Fe^{3+} (0.55 Å) ions have ionic radii close to or in the reasonable difference to that of Zn^{2+} cation (0.74 Å) which can facilitate the single doping or multi-doping. The electronic configurations of Fe and Mn ions contain many unpaired electrons and possess high ability to improve the magnetic properties. Besides enhancing the optical performance, accruing remarkable magnetic properties in ZnO can support its multi-functionality in spintronics or medical applications. As a result, it is expected for ZnO that Li monodoping and (Li, Mn) or (Li, Fe) dual doping can enhance the optical, catalytic, and magnetic properties. Herein, high-purity nanopowders of ZnO, $\text{Zn}_{0.97}\text{Li}_{0.03}\text{O}$, $\text{Zn}_{0.94}\text{Li}_{0.03}\text{Mn}_{0.03}\text{O}$, and $\text{Zn}_{0.94}\text{Li}_{0.03}\text{Fe}_{0.03}\text{O}$ were synthesized by coprecipitation method. The magnetic properties (M-H curves) of the synthesized powders were measured at room temperature.

2 Synthesis, Characterization, and Measurements

High-purity powders of Li monodoped and (Li, Mn) or (Li, Fe) codoped ZnO nanoparticles were synthesized by simple coprecipitation technique using NaOH as base. $\text{Zn}(\text{CH}_3\text{COO})_2 \cdot 2\text{H}_2\text{O}$ (99.9%), LiCl (99.8%), $\text{MnCl}_2 \cdot 2\text{H}_2\text{O}$ (99.7%), and $\text{Fe}(\text{NO}_3)_3 \cdot 9\text{H}_2\text{O}$ (99.7%) as starting materials were used to prepare the different compositions. Pure ZnO, $\text{Zn}_{0.97}\text{Li}_{0.03}\text{O}$, $\text{Zn}_{0.94}\text{Li}_{0.03}\text{Mn}_{0.03}\text{O}$, and $\text{Zn}_{0.94}\text{Li}_{0.03}\text{Fe}_{0.03}\text{O}$ compositions were synthesized by dissolving appropriate weights of starting materials in deionized water (H_2O) under continuous stirring for 60 min. Strong NaOH solution was added dropwise to these solutions with continuous stirring until pH is equal to 8 to form the corresponding hydroxide precipitates. The deionized H_2O was used to wash the obtained precipitates for many times. The formed precipitates were dried, ground to fine powders, and then calcined at 500 °C for 3 h to yield the desired ZnO compositions. X-ray diffraction analysis (XRD, PANalytical X-ray diffraction equipment model X'Pert Pro) and least-square refined technique (Maud software) are used to investigate the crystal structure, lattice constant, and crystallite size of the synthesized samples. Fourier-transform infrared (FT-IR) spectra of pure, Li doped, and (Li, Mn) or (Li, Fe) codoped ZnO nanopowders were recorded using a Fourier transform infrared spectrometer (JASCO, model 4600). The size and shape of the synthesized particles were found by using a transmission electron microscope (TEM, JEOL JEM-2100). The optical properties and the band gap energy were analyzed by using a double-beam spectrophotometer-JASCO

(model V-570 UV-Vis-NIR). The magnetic properties of pure, Li doped, and (Li, Mn) or (Li, Fe) codoped ZnO nanostructures were identified using a vibrating sample magnetometer (VSM, Lake Shore Model 7410).

3 Results and Discussion

3.1 Crystal Structure Studies

Figure 1 depicts the X-ray diffraction patterns of pure, Li monodoped, and (Li, Mn) and (Li, Fe) codoped ZnO powders synthesized by the coprecipitation method. All the diffraction peaks can be exactly indexed to ZnO with a hexagonal wurtzite structure (JCPDS. No: 36–1451, space group: p63mc). Each pattern contains nine peaks that have similar relative intensities assigned to the (100), (002), (101), (102), (110), (103), (200), (112), and (201) crystallographic planes of the ZnO phase. There are no peaks related to any impurities or secondary phases in these patterns, signifying their high purity. Figure 2 demonstrates the enlarged pattern of the highest diffraction peak corresponding to the (101) plane of all ZnO compositions. It can be seen that the intensity of the main peak of ZnO is enhanced due to Li monodoping and somewhat was decreased after (Li, Mn) and (Li, Fe) codoping. Besides that, the position of the peak is shifted towards a higher angle for Li monodoping and towards a lower 2θ angle for (Li, Mn) and (Li, Fe) codoping. The changes in the position and intensity of the (101) plane suggest that the crystal parameters and crystallinity of ZnO are affected due to incorporation of Li^+ , Mn^{2+} , or Fe^{3+} ions which possess different ionic radii compared to Zn^{2+}

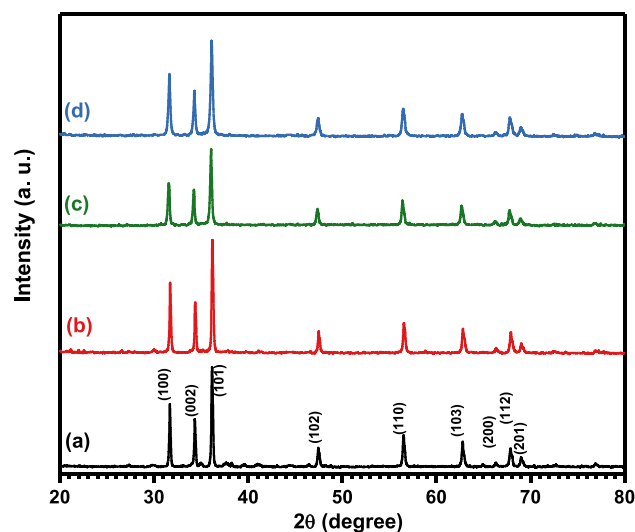


Fig. 1 XRD patterns of **a** pure ZnO, **b** $\text{Zn}_{0.97}\text{Li}_{0.03}\text{O}$, **c** $\text{Zn}_{0.94}\text{Li}_{0.03}\text{Mn}_{0.03}\text{O}$, and **d** $\text{Zn}_{0.94}\text{Li}_{0.03}\text{Fe}_{0.03}\text{O}$ samples synthesized by the coprecipitation method

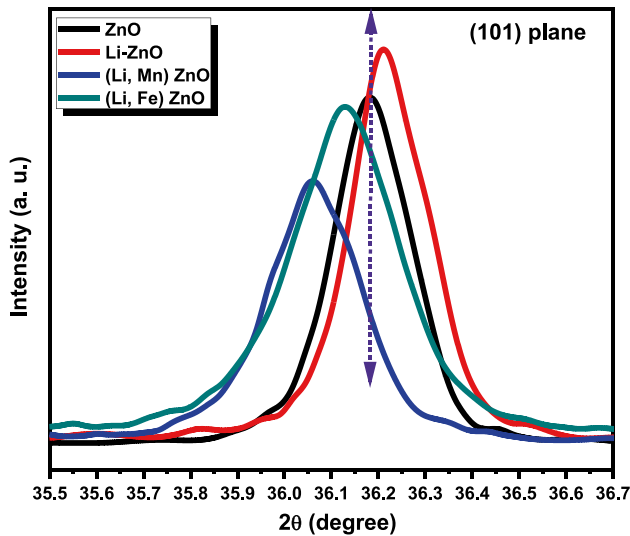


Fig. 2 Influence of Li monodoping and (Li, Mn) and (Li, Fe) codoping on position and intensity of (101) main plane of ZnO structure

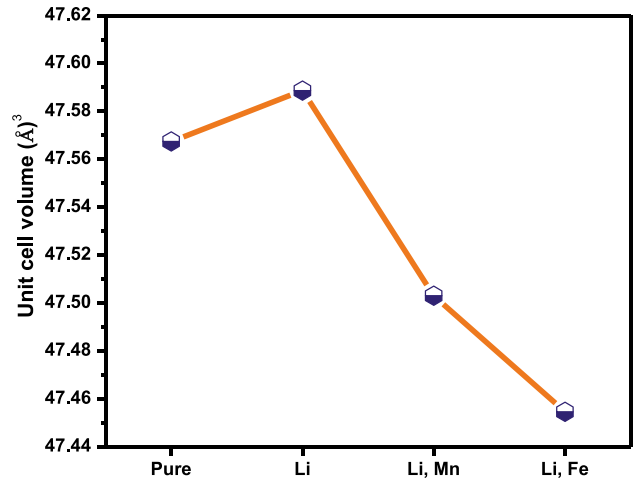


Fig. 3 Effect of Li monodoping and (Li, Mn) and (Li, Fe) codoping on unit cell volume of nanocrystalline ZnO structure

cations. The phase purity, lattice constant (a , c), and unit cell volume of undoped ZnO, $Zn_{0.97}Li_{0.03}O$, $Zn_{0.94}Li_{0.03}Mn_{0.03}O$, and $Zn_{0.94}Li_{0.03}Fe_{0.03}O$ nanopowders were estimated based on least-square Rietveld refinement analysis using Maud software (Table 1). As well, the changes in lattice constant of ZnO were used to analyze and ensure the effective incorporation of Li^+ , Mn^{2+} , or Fe^{3+} ions into ZnO host lattice. As shown in Fig. 3 and Table 1, notable increases in lattice parameters and unit cell volume of ZnO are observed due to Li ion doping. This behavior can be attributed to the substitution of Zn^{2+} ions (0.74 \AA-VI) by Li^+ ions (0.78 \AA-VI) with larger ionic radius [24]. On the other hand, insertion of Mn^{2+} or Fe^{3+} ions plus Li^+ ions into the ZnO lattice significantly reduces the lattice parameters and unit cell volume of ZnO especially in case of the Fe dopant. Both Mn^{2+} ions (0.67 \AA-VI) and Fe^{3+} (0.55 \AA-VI) ions have ionic radii smaller than that of Zn^{2+} cations (0.74 \AA-VI), and hence, it is expected that the incorporation of both ions will decrease the lattice parameters and unit cell volume of ZnO particularly with Fe ions [25]. These results confirm that Li^+ , Mn^{2+} , and Fe^{3+} ions are really incorporated into the ZnO lattice. The crystallite sizes (D) of prepared samples were calculated by using the Scherrer equation, $D = K\lambda/\beta \cdot \cos\theta$ [26]. The measured crystallite size of the pure ZnO is estimated to be

35 nm. In the case of the $Zn_{0.97}Li_{0.03}O$, $Zn_{0.94}Li_{0.03}Mn_{0.03}O$, and $Zn_{0.94}Li_{0.03}Fe_{0.03}O$ samples, the crystallite size was found to be 33 nm, 29 nm and 26 nm, respectively. It can be noticed that the addition of Mn^{2+} or Fe^{3+} clearly reduces the crystallite size and limit the particles growth.

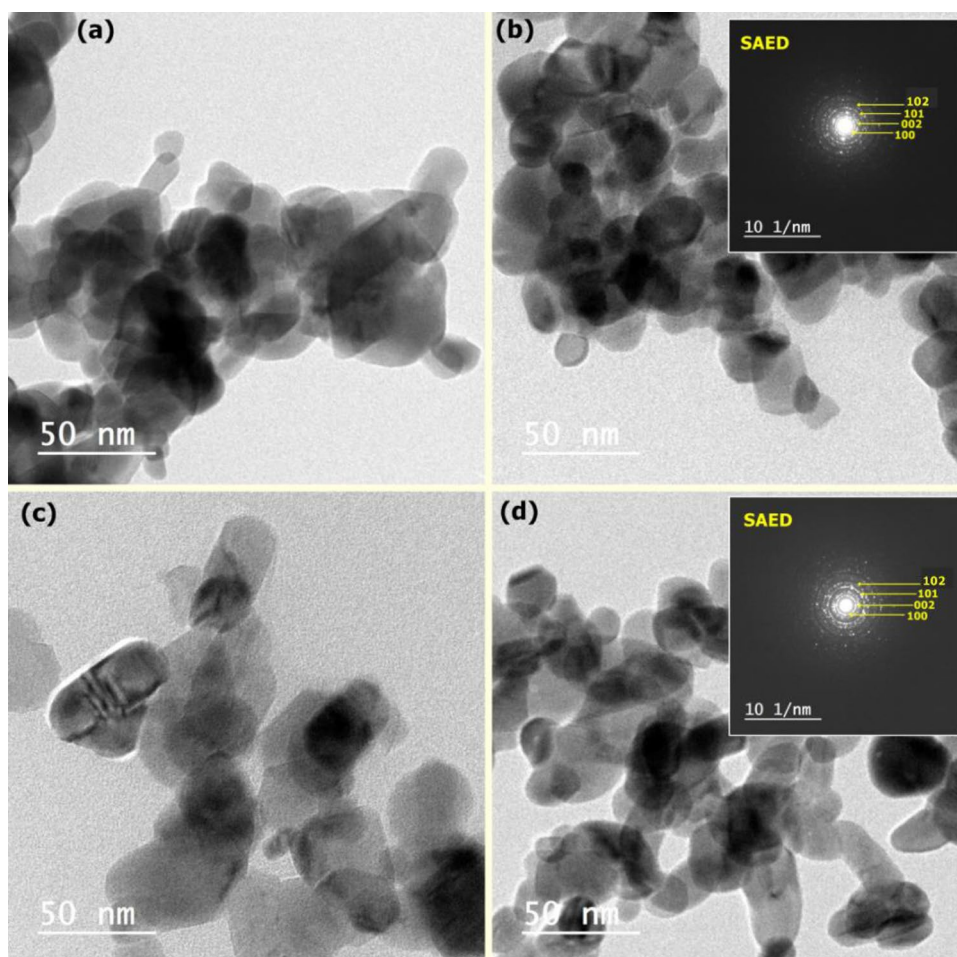
3.2 TEM: Particle Size and Shape

The morphology and particle size of the pure, Li monodoped, and (Li, Mn) and (Li, Fe) codoped ZnO powders were investigated by transmission electron microscopy (TEM) as illustrated in Fig. 4. Pure ZnO powders show asymmetrical nanoparticles with a certain degree of agglomeration and approximately have an average particle size of 37 nm. The TEM image of Li monodoped ZnO powders displays uniform spherical nanoparticles with less agglomeration, and the average particle size was reduced to 35 nm. The image of the (Li, Mn) codoped ZnO sample illustrates that the particles of the ZnO are transformed to elongated shapes without agglomeration with an average particle size of 32 nm. In case of (Li, Fe) codoped ZnO powders, the image clearly shows a mixture of uniform nanospherical and elongated particles with a small average particle size of 27 nm. It seems that the presence of Mn^{2+} or Fe^{3+} ions restricts the growth of ZnO particles in accordance

Table 1 Crystallite size D (nm), lattice parameters (a , c), lattice parameter ratio (c/a), unit cell volume (V), and band gap of pure, Li doped, and (Li, Mn) and (Li, Fe) codoped ZnO

Samples	D (nm)	a (Å)	c (Å)	c/a	V (Å ³)	Band gap (eV)
ZnO	35	3.2488	5.2041	1.6018	47.5674	3.2
Li	33	3.2494	5.2045	1.6016	47.5886	3.203
Li, Mn	29	3.2471	5.2025	1.6020	47.5036	3.14
Li, Fe	26	3.2461	5.2004	1.6021	47.4546	3.17

Fig. 4 TEM images of **a** pure ZnO, **b** $\text{Zn}_{0.97}\text{Li}_{0.03}\text{O}$, **c** $\text{Zn}_{0.94}\text{Li}_{0.03}\text{Mn}_{0.03}\text{O}$, and **d** $\text{Zn}_{0.94}\text{Li}_{0.03}\text{Fe}_{0.03}\text{O}$ nanopowders, selected area electron diffraction (SAED) inset image



with XRD data. The selected area electron diffraction patterns (SAED, inset Fig. 4) of Li monodoped and (Li, Fe) codoped ZnO nanoparticles obviously display strong diffraction rings ascribed to the (100), (022), (101), and (102) crystallographic planes which confirm the high crystallinity of doped and binary doped ZnO samples.

3.3 Band Gap and Electromagnetic Absorption

The UV–Vis DRS spectra of ZnO, $\text{Zn}_{0.97}\text{Li}_{0.03}\text{O}$, $\text{Zn}_{0.94}\text{Li}_{0.03}\text{Mn}_{0.03}\text{O}$, and $\text{Zn}_{0.94}\text{Li}_{0.03}\text{Fe}_{0.03}\text{O}$ nanopowders are presented in Fig. 5. Pure ZnO exhibits a strong absorption below a wavelength of 400 nm which corresponds to its band gap energy absorption. In a Li monodoped ZnO structure, a significant increase in the intensity of the diffuse reflectance due to the insertion of Li ions into the ZnO lattice was observed. As well, the absorption edge becomes sharper which is a dynamic factor in optoelectronic applications such as solar cell; the sharpness of the absorption edge means more charge carriers in the conduction band [27]. The diffuse reflectance of $\text{Zn}_{0.94}\text{Li}_{0.03}\text{Mn}_{0.03}\text{O}$ and $\text{Zn}_{0.94}\text{Li}_{0.03}\text{Fe}_{0.03}\text{O}$ nanopowders shows gradual increases

in the absorption within wavelengths of 650–400 nm with red shifts of absorption edge above 400 nm. The

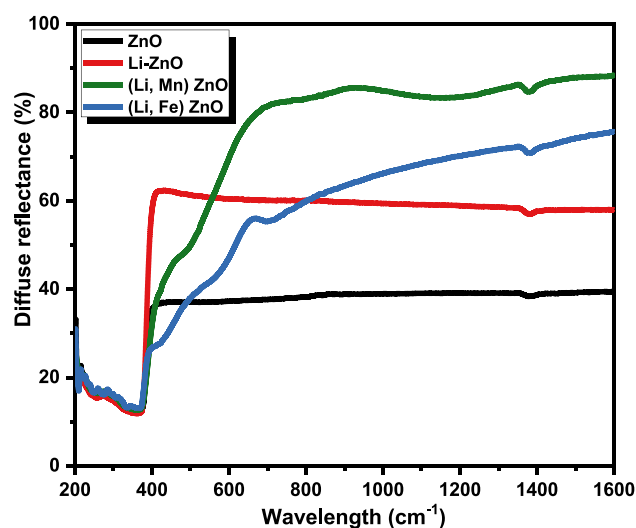


Fig. 5 Diffuse reflectance spectra of pure, Li monodoped and (Li, Mn) and (Li, Fe) codoped ZnO powders

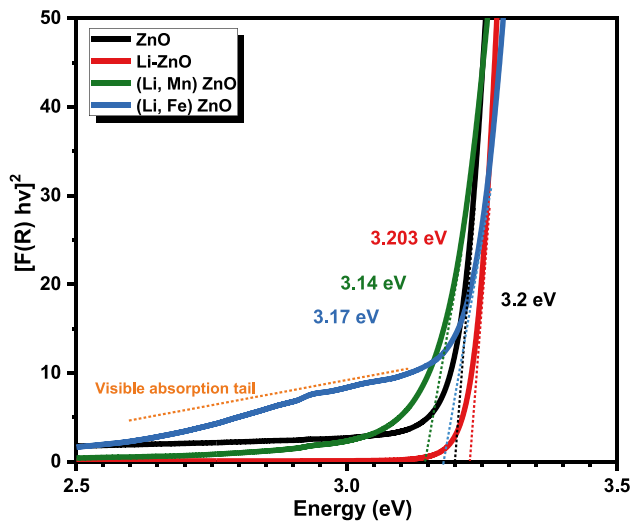


Fig. 6 Optical band gap of pure, Li monodoped and (Li, Mn) and (Li, Fe) codoped ZnO nanopowders

optical band gap energy of pure, Li doped, and (Li, Mn) and (Li, Fe) codoped ZnO powders is determined using the Kubelka–Munk equation [28], $[F(R) hv]^2$ versus $h\nu$ (eV), where $h\nu$ is the photon energy in eV as demonstrated in Fig. 6. The band gap is determined by extrapolating and intersecting the linear portion of $[F(R) hv]^2$ to cut the energy axis ($h\nu$). The calculated band gap energy of ZnO, $Zn_{0.97}Li_{0.03}O$, $Zn_{0.94}Li_{0.03}Mn_{0.03}O$, and $Zn_{0.94}Li_{0.03}Fe_{0.03}O$ comes out to be 3.2 eV (388 nm), 3.203 eV (387 nm), 2.98 eV (394 nm), and 2.97 eV (391 nm), respectively. As illustrated in Fig. 6, it can be noticed that the absorption profile of $Zn_{0.94}Li_{0.03}Fe_{0.03}O$ nanopowders has a clear long tail that extends over the entire visible range. The reduction in the optical band gap energy of $Zn_{0.94}Li_{0.03}Mn_{0.03}O$ and $Zn_{0.94}Li_{0.03}Fe_{0.03}O$ can be attributed to the formation of new defect levels due to the impurity atoms [27, 29]. Introducing of Mn^{2+} and Fe^{3+} ions plus Li^+ causes contraction of the ZnO band gap due to the s-d and p-d exchange interactions between the conduction band of ZnO (involving the 4 s of Zn and 2 s of O) and the 3d electrons of Mn^{2+} and Fe^{3+} ions [30, 31].

3.4 FTIR Technique

Figure 7 shows the FTIR spectra of pure, Li doped, and (Li, Mn) and (Li, Fe) codoped ZnO powders synthesized by the coprecipitation method in wavenumber of 400–4000 cm^{-1} . Similar FTIR profiles were detected in all ZnO compositions. The two bands located at approximately 3446 cm^{-1} and 1633 cm^{-1} can be assigned to stretching and bending vibration modes of the adsorbed water molecules (H_2O) [32, 33]. The weak absorption bands situated at 2920 cm^{-1} and 2860 cm^{-1} are attributed to the vibrations of the C–H

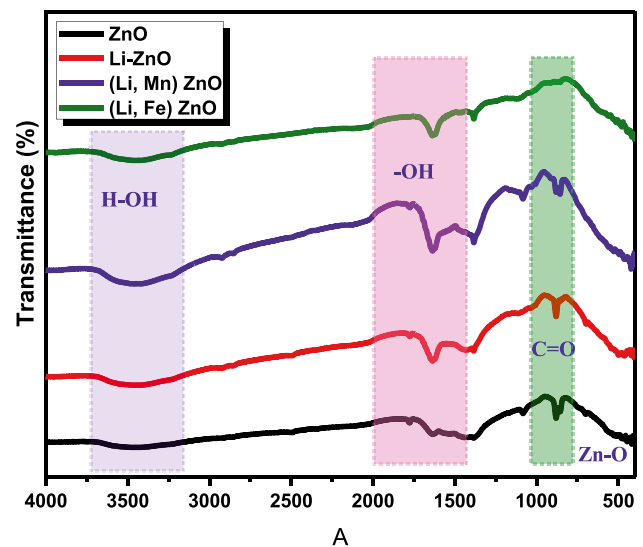


Fig. 7 FTIR spectra of a pure ZnO, b Li doped, c (L, Mn), and d (Li, Fe) codoped ZnO samples

group while the small absorption bands located at 1083 cm^{-1} and 881 cm^{-1} are assigned to the stretching vibration of the C=O group of minor non-decomposed acetate on the ZnO surface [34, 35]. The characteristic absorption band of the ZnO structure can be seen in the wavelength of 400–500 cm^{-1} , which represents the stretching vibration mode of the Zn–O bond [32, 33]. The characteristic vibrational mode of pure ZnO is closely situated at 452 cm^{-1} . The position of this characteristic absorption band is shifted to 442 cm^{-1} , 435 cm^{-1} , and 432 cm^{-1} in $Zn_{0.97}Li_{0.03}O$, $Zn_{0.94}Li_{0.03}Mn_{0.03}O$, and $Zn_{0.94}Li_{0.03}Fe_{0.03}O$ samples, respectively. These shifts to lower wavenumber can be attributed to the substitution of Zn^{2+} cation in the ZnO host lattice by Li^+ , Mn^{2+} , and Fe^{3+} ions, which somewhat perturbed the bond strength of the Zn–O–Zn network and influence on position of the absorption band.

3.5 Magnetic Property Analysis

Figure 8 depicts the room temperature magnetization versus magnetic field hysteresis loops of ZnO, $Zn_{0.97}Li_{0.03}O$, $Zn_{0.94}Li_{0.03}Mn_{0.03}O$, and $Zn_{0.94}Li_{0.03}Fe_{0.03}O$ nanoparticles in the switchable magnetic field of ± 20 KOe. Pure ZnO nanopowders reveal a diamagnetic performance but with mild hysteresis at low magnetic field. The diamagnetic behavior can be ascribed to the diamagnetic nature of the particle core while the small hysteresis shape may be attributed to defects and uncompensated spins at the surface [18, 36]. Interestingly, the $Zn_{0.94}Li_{0.03}Fe_{0.03}O$ composition exhibits superparamagnetic behavior at room temperature; it obviously shows a semi-saturation magnetization of 0.02 emu/g but having a nearly zero remnant magnetization and coercivity (7 Oe).

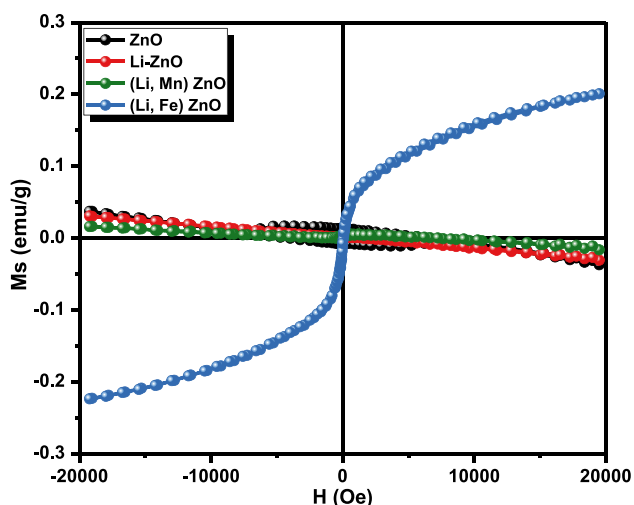


Fig. 8 Magnetic properties of pure, Li monodoped and (L, Mn) and (Li, Fe) codoped ZnO nanopowders

This performance is the clear indication of room temperature superparamagnetism of the $\text{Zn}_{0.94}\text{Li}_{0.03}\text{Fe}_{0.03}\text{O}$ structure. Similarly to pure ZnO nanopowders, both $\text{Zn}_{0.97}\text{Li}_{0.03}\text{O}$ and $\text{Zn}_{0.94}\text{Li}_{0.03}\text{Mn}_{0.03}\text{O}$ samples display a diamagnetic curve. Based on our experimental results, the changes in unit cell volume, band gap energy, and FTIR absorption bands confirm the effective incorporation of Li^+ , Mn^{2+} , or Fe^{3+} ions into the ZnO host lattice. Besides that, the XRD pattern and HRTEM image ruled out the presence of any secondary phases or magnetic clusters especially in the $\text{Zn}_{0.94}\text{Li}_{0.03}\text{Fe}_{0.03}\text{O}$ structure. The synthesis of the (Li, Fe) codoped ZnO structure was carried out in air atmosphere (oxygen) at 500 °C for 3 h which prevents the formation of the metallic Fe. Furthermore, Li^+ (0.78 Å) and Fe^{3+} (0.55 Å) ions have ionic radii close to or in the reasonable difference to that of Zn^{2+} cation (0.74 Å) which can facilitate the multi-doping process. Based on these observations, we can conclude that the superparamagnetic performance of the $\text{Zn}_{0.94}\text{Li}_{0.03}\text{Fe}_{0.03}\text{O}$ sample originates from intrinsic nature and not related to any impurities. The crystallite size (XRD) and particle size (TEM) measurements revealed that the $\text{Zn}_{0.94}\text{Li}_{0.03}\text{Fe}_{0.03}\text{O}$ sample possesses the lowest crystallite size (26 nm) and particle size (27 nm) compared to the other samples. The small particle size of $\text{Zn}_{0.94}\text{Li}_{0.03}\text{Fe}_{0.03}\text{O}$ powder means that it has a large surface area with more oxygen vacancies which can support the magnetic interaction. According to the Ruderman–Kittel–Kasuya–Yosida (RKKY) theory [15], the magnetism can be attributed to the exchange interaction between localized spin-polarized electrons and the conductive electrons. This exchange interaction can lead to the spin polarization of the conductive electrons. Consequently, the spin-polarized conductive electrons can make an exchange interaction with local spin-polarized electrons of other Fe^{3+} ions. Thus, after the long-range exchange interaction, almost

all Fe^{3+} ions exhibit the same spin direction. The conductive electrons are regarded as a media to contact all Fe^{3+} ions. As a result, the sample exhibits superparamagnetic behaviors at room temperature. Also, the room temperature superparamagnetic behavior in nanocrystalline (Li, Fe) codoped ZnO can be explained by the existence of two types of magnetic state [37]. The first type is the ferromagnetic performance originating from the oxygen vacancies, and the second type is the antiferromagnetic behavior inducing from the Fe–Fe ion interaction. It seems that the antiferromagnetic state suppresses the ferromagnetism couplings, resulting in a rapid decrease in magnetic moment. The instantaneous presence of both ferromagnetism and antiferromagnetism gives rise to a disordered state of superparamagnetism. Hence, $\text{Zn}_{0.94}\text{Li}_{0.03}\text{Fe}_{0.03}\text{O}$ nanoparticles display the room temperature.

4 Conclusions

Robust superparamagnetic behavior has been achieved in $\text{Zn}_{0.94}\text{Li}_{0.03}\text{Fe}_{0.03}\text{O}$ nanoparticles within a magnetic field of $\pm 20,000$ Oe. High-purity ZnO, $\text{Zn}_{0.97}\text{Li}_{0.03}\text{O}$, $\text{Zn}_{0.94}\text{Li}_{0.03}\text{Mn}_{0.03}\text{O}$, and $\text{Zn}_{0.94}\text{Li}_{0.03}\text{Fe}_{0.03}\text{O}$ nanostructures were synthesized by means of the coprecipitation method. The XRD analysis confirmed the single-phase nature of all synthesized compositions and the alterations of the lattice constant established for effective monodoping and dual doping. Extending of the optical band gap of ZnO to the visible region via ion codoping can be useful in the photocatalytic applications. Interestingly, the $\text{Zn}_{0.94}\text{Li}_{0.03}\text{Fe}_{0.03}\text{O}$ composition exhibits superparamagnetic behavior at room temperature; it clearly shows a semi-saturation magnetization of 0.02 emu/g but having nearly zero remnant magnetization and coercivity.

References

1. Raizada, P., Sudhaik, A., Patial, S., Hasija, V., Khan, A.A.P., Singh, P., Gautam, S., Kaur, M., Nguyen, V.-H.: Engineering nanostructures of CuO-based photocatalysts for water treatment: Current progress and future challenges. *Arab. J. Chem.* **13**, 8424–8457 (2020)
2. Bousslama, W., Elhouichet, H., Férid, M.: Enhanced photocatalytic activity of Fe doped ZnO nanocrystals under sunlight irradiation. *Optik* **134**, 88–98 (2017)
3. Kazmi, J., Ooi, P.C., Goh, B.T., Lee, M.K., Wee, M.F.M.R., Karim, S.S.A., Razad, S.R.A., Mohamed, M.A.: Bi-doping improves the magnetic properties of zinc oxide nanowires. *RSC Adv.* **10**, 23297–23311 (2020)
4. Punnoose, A., Reddy, K.M., Hays, J., Thurber, A., Engelhard, M.H.: Magnetic gas sensing using a dilute magnetic semiconductor. *Appl. Phys. Lett.* **89**, 112509 (2006)
5. Kayani, Z.N., Bashir, H., Riaz, S., Naseem, S.: Optical properties and antibacterial activity of V doped ZnO used in solar cells and biomedical applications. *Mater. Res. Bull.* **115**, 121–129 (2019)
6. Liu, H., Li, G.P., Xu, D.J.E.N.N., Lin, Q.L., Gao, X.D., Wang, C.L.: Room temperature ferromagnetism in D-D neutron

- irradiated ZnO single crystals. *J Supercond Nov Magn.* **33**, 1535–1542 (2020)
7. Yaseen, M., Ambreen, H., Zia, M., Javed, H.M.A., Mahmood, A., Murtaza, A.: Study of half metallic ferromagnetism and optical properties of Mn-doped CdS. *J. Supercond. Novel Magn.* **34**, 135–141 (2021)
 8. Sharma, K.R., Negi, N.S.: Doping effect of cobalt on various properties of nickel oxide prepared by solution combustion method. *J. Supercond. Novel Magn.* **34**, 633–645 (2021)
 9. de Santana, W.M.O.S., Caetano, B.L., de Annunzio, S.R., Pulcinelli, S.H., Ménager, C., Fontana, C.R., Santilli, C.V.: Conjugation of superparamagnetic iron oxide nanoparticles and curcumin photosensitizer to assist in photodynamic therapy. *Colloids and Surfaces B: Biointerfaces* **196**, 111297 (2020)
 10. Rosowska, J., Kaszewski, J., Witkowski, B., Wachnicki, Ł., Kuryliszyn-Kudelska, I., Godlewski, M.: The effect of iron content on properties of ZnO nanoparticles prepared by microwave hydrothermal method. *Optical Materials* **109**, 110089 (2020)
 11. Look, D.C.: Recent advances in ZnO materials and devices. *Mater. Sci. Eng., B* **80**, 383–387 (2001)
 12. Kumar, S., Kumar, M., Kumar, A., Sharma, S., Shahi, P., Chatterjee, S., Ghosh, A.K.: Investigations on structural and optical properties of Al-modified ZnO nanoparticles. *J. Mater. Sci.: Mater. Electron.* **31**, 7715–7723 (2020)
 13. Peter, I.J., Praveen, E., Vignesh, G., Nithiananthi, P.: ZnO nanostructures with different morphology for enhanced photocatalytic activity. *Mater. Res. Express* **4**, 124003 (2017)
 14. Yakout, S.M., El-Sayed, A.M.: Synthesis, structure, and room temperature ferromagnetism of Mn and/or Co doped ZnO nanocrystalline. *J Supercond Nov Magn* **29**, 1593–1599 (2016)
 15. Wang, J., Wan, J., Chen, K.: Facile synthesis of superparamagnetic Fe-doped ZnO nanoparticles in liquid polyols. *Mater. Lett.* **64**, 2373–2375 (2010)
 16. Mukherjee, S., Liang, L., Veiseh, O.: Recent advancements of magnetic nanomaterials in cancer therapy. *Pharmaceutics* **12**, 147 (2020)
 17. Vettumperumal, R., Kalyanaraman, S., Santoshkumar, B., Thangavel, R.: Magnetic properties of high Li doped ZnO sol–gel thin films. *Mater. Res. Bull.* **50**, 7–11 (2014)
 18. Ahmed, S.A.: Structural, optical, and magnetic properties of Mn-doped ZnO samples. *Results in Physics* **7**, 604–610 (2017)
 19. Beltrán, J.J., Barrero, C.A., Punnoose, A.: Understanding the role of iron in the magnetism of Fe doped ZnO nanoparticles. *Phys. Chem. Chem. Phys.* **17**, 15284–15296 (2015)
 20. Duan, J., Wang, H., Wang, H., Zhang, J., Wu, S., Wang, Y.: Mn-doped ZnO nanotubes: from facile solution synthesis to room temperature ferromagnetism. *Cryst Eng Comm* **14**, 1330–1336 (2012)
 21. Djerdj, I., Garnweitner, G., Arcon, D., Pregelj, M., Jaglicic, Z., Niederberger, M.: Diluted magnetic semiconductors: Mn/Co-doped ZnO nanorods as case study. *J. Mater. Chem.* **18**, 5208–5217 (2008)
 22. Zulfiqar, M., Zubair, A., Khan, T., Hua, N., Ilyas, S., Fashu, A.M., Afzal, M.A., Safeen, R., Khan. Oxygen vacancies induced room temperature ferromagnetism and enhanced dielectric properties in Co and Mn co-doped ZnO nanoparticles. *J Mater Sci: Mater Electron* **32**, 9463–9474 (2021)
 23. Tariq, M., Li, Y., Li, W., Yu, Z., Li, J., Hu, Y., Zhu, M., Jin, H., Li, Y., Skotnicova, K.: Enhancement of ferromagnetic properties in (Fe, Ni) co-doped ZnO flowers by pulsed magnetic field processing. *J. Mater. Sci.: Mater. Electron.* **30**, 8226–8232 (2019)
 24. Shawuti, S., Sherwani, A.R., Can, M.M., Gülgün, M.A.: Complex impedance analyses of Li doped ZnO electrolyte materials. *Sci. Rep.* **10**, 8228 (2020)
 25. Elilarassi, R., Chandrasekaran, G.: Optical, electrical and ferromagnetic studies of ZnO: Fe diluted magnetic semiconductor nanoparticles for spintronic applications. *Spectrochim. Acta Part A Mol. Biomol. Spectrosc.* **186**, 120–131 (2017)
 26. Akbarian, M., Mahjoub, S., Elahi, S.M., Zabih, E., Tashakkorian, H.: *Urtica dioica* L. extracts as a green catalyst for the biosynthesis of zinc oxide nanoparticles: characterization and cytotoxic effects on fibroblast and MCF-7 cell lines. *New J. Chem.* **42**, 5822–5833 (2018)
 27. Sandeep, K.M., Bhat, S., Serrao, F.J., Dharmaprasanth, S.M.: Li doped ZnO thin films for optoelectronic applications. *AIP Conference Proceedings* **1731**, 080055 (2016)
 28. Uddin, M.T., Hoque, M.E., Bhoumick, M.C.: Facile one-pot synthesis of heterostructure SnO₂/ZnO photocatalyst for enhanced photocatalytic degradation of organic dye. *RSC Adv.* **10**, 23554–23565 (2020)
 29. Bhatt, A.S., Ranjitha, R., Santosh, M.S., Ravikumar, C.R., Prashantha, S.C., Maphanga, R.R., Lenz e Silva, G.F.B.: Optical and electrochemical applications of Li-doped NiO nanostructures synthesized via facile microwave technique. *Materials* **13**, 2961 (2020)
 30. López-Suárez, A., Acosta, D., Magaña, C., Hernández, F.: Optical, structural and electrical properties of ZnO thin films doped with Mn. *J. Mater. Sci.: Mater. Electron.* **31**, 7389–7397 (2020)
 31. Srinivasulu, T., Saritha, K., Reddy, K.T.R.: Synthesis and characterization of Fe-doped ZnO thin films deposited by chemical spray pyrolysis. *Modern Electronic Materials* **3**, 76–85 (2017)
 32. Rezende, C.P., da Silva, J.B., Mohallem, N.D.S.: Influence of drying on the characteristics of zinc oxide nanoparticles. *Braz. J. Phys.* **39**, 248–251 (2009)
 33. Thi, T.U.D., Nguyen, T.T., Thi, Y.D., Thi, K.H.T., Phan, B.T., Pham, K.N.: Green synthesis of ZnO nanoparticles using orange fruit peel extract for antibacterial activities. *RSC Adv.* **10**, 23899–23907 (2020)
 34. Shamhari, N.M., Wee, B.S., Chin, S.F., Kok, K.Y.: Synthesis and characterization of zinc oxide nanoparticles with small particle size distribution. *Acta Chim. Slov.* **65**, 578–585 (2018)
 35. Largani, S.H., Pasha, M.A.: The effect of concentration ratio and type of functional group on synthesis of CNT–ZnO hybrid nanomaterial by an in situ sol–gel process. *Int Nano Lett* **7**, 25–33 (2017)
 36. Yakout, S.M.: Pure and Gd-based Li, Na, Mn or Fe codoped ZnO nanoparticles: Insights into the magnetic and photocatalytic properties. *Solid State Sci.* **83**, 207–217 (2018)
 37. Mohapatra, J., Mishra, D.K., Singh, S.K.: Superparamagnetic behavior in chemically synthesized nanocrystalline Zn_{0.99}Ni_{0.01}O powders. *Materials Letters* **75**, 91–94 (2012)

Publisher's Note Springer Nature remains neutral with regard to jurisdictional claims in published maps and institutional affiliations.